

# Detection of DCI by multiphoton ionization and determination of DCI and HCl internal state distributions

Paul J. Dagdigian and David F. Varley<sup>a)</sup>

*Department of Chemistry, The Johns Hopkins University, Baltimore, Maryland 21218-2685*

Rohana Liyanage<sup>b)</sup> and Robert J. Gordon

*Department of Chemistry, University of Illinois at Chicago (m/c 111), Chicago, Illinois 60607-7061*

Robert W. Field

*Department of Chemistry, Massachusetts Institute of Technology, Cambridge, Massachusetts 02139*

(Received 28 June 1996; accepted 5 September 1996)

A study of the 2+1 resonantly enhanced multiphoton ionization (REMPI) spectrum of DCI is reported. Transition energies for excitation of the  $F^1\Delta-X^1\Sigma^+$  (0,0) and (1,0) bands, as well as the  $V^1\Sigma^+-X^1\Sigma^+(v',0)$  bands, for  $v'=15-19$ , are presented. The derived molecular constants for the  $F-X$  (0,0) and the  $V-X$  bands agree well with those previously obtained from analysis of the one-photon VUV absorption spectrum [A. E. Douglas and F. R. Greening, *Can. J. Phys.* **57**, 1650 (1979)]. The ion signals for excitation through various rotational lines in the  $E-X$  (0,0) and  $F-X$  (0,0) and (1,0) bands are compared with theoretical two-photon line strengths. Extensive power- and  $J'$ -dependent ion fragmentation is observed for the former band. No fragmentation is observed in the  $F-X$  bands; however, the ion signal strengths are found to vary strongly with  $J'$ . This variation of REMPI signal strengths vs  $J'$  was shown to be due to an indirect predissociation, as in HCl. Tables of experimental line strength factors for the  $F-X$  (0,0) and (1,0) bands of HCl and DCI are reported. Finally, the relative REMPI detection sensitivities for HCl and DCI, through their respective  $F-X$  (0,0)  $R(1)$  lines, are compared. © 1996 American Institute of Physics. [S0021-9606(96)02046-6]

## I. INTRODUCTION

Resonantly enhanced multiphoton ionization<sup>1</sup> (REMPI) is a very sensitive spectroscopic tool which has been used in studies of both the spectroscopy and reaction dynamics of small molecules in the gas phase. In contrast to the more frequently employed method of laser-induced fluorescence, the use of REMPI to obtain relative populations of different internal states is problematic.<sup>2-5</sup> In part, the determination of populations requires care because of the ease of saturating the resonant transition, which can cause the dependence of the ionization rate on the laser power to vary from level to level.<sup>6</sup> In addition, there is the possibility that the resonantly excited state is perturbed; such perturbations can have large effects on the rotational intensity factors.<sup>4,5</sup> This is, in fact, quite likely to occur in REMPI detection because of the high density of electronic states at energies reached by the absorption of two or three UV photons. Lastly, dissociation may compete with ionization of either the intermediate or a superexcited state, and both parent and fragment ions can be produced; this leads to further complications in converting ion signals to relative internal state populations.<sup>3,7</sup> Since it is difficult to calculate quantitatively the effects of all these factors on the magnitude of an ion signal, it is useful to

calibrate the REMPI signal strengths by using a sample with a known internal state distribution, such as a Boltzmann distribution at a known temperature.<sup>3,4,7,8</sup>

Sensitive, state-selective detection of HCl by the REMPI technique has been extensively employed in studies of the dynamics of a number of collisional processes involving this molecule, including rotational energy transfer,<sup>9,10</sup> photodissociation,<sup>11-14</sup> coherent control,<sup>15</sup> chemical reaction,<sup>16-20</sup> and surface scattering.<sup>21,22</sup> The HCl molecule provides a very good example of the complications in REMPI detection owing to both perturbations and dissociation. Two of the strongest transitions in the 2+1 REMPI spectrum of HCl involve resonant excitation to the  $E^1\Sigma^+$  and  $F^1\Delta$  electronic states.<sup>23,24</sup> These transitions have proven to be very useful for the determination of HCl rovibrational populations. For the  $E-X$  transition, considerable ion fragmentation occurs, and  $H^+$  and  $Cl^+$  ions are formed with intensities comparable to those of the parent molecular ion at typical laser power densities.<sup>3,24,25</sup> Moreover, the detection sensitivity for excitation through both the  $v'=0$  and 1 vibrational levels drops significantly with increasing rotational angular momentum,  $J'$ . In contrast, there is no fragmentation for ionization through the  $F-X$  transition. However, the REMPI line strength factors vary strongly with  $J'$  for ionization through both the  $F^1\Delta$   $v'=0$  and 1 levels.<sup>4</sup> This variation in intensity has been shown to be due to a loss mechanism that is the result of an indirect predissociation of the  $F^1\Delta$  state.<sup>5</sup>

As a result of recent collisional experiments, in which both HCl and DCI internal state distributions are reported,

<sup>a)</sup>Present address: Stanford Research Systems, 1290-D Reamwood Ave., Sunnyvale, California 94089.

<sup>b)</sup>Present address: Department of Chemistry, University of Utah, Salt Lake City, Utah 84112.

there is a need to quantify the REMPI detection of the DCI isotopomer. In the present paper, we report DCI REMPI spectra and intensity factors for ionization through the  $E\ ^1\Sigma^+$  and  $F\ ^1\Delta$  states. As with the corresponding transition in HCl, we observe considerable formation of atomic ions from the  $E$  state. In addition, we directly compare the REMPI signals for detection of HCl and DCI through their respective  $F$  states. We also show that the  $J'$ -dependence of the  $F-X$  transition of DCI can be satisfactorily explained by an indirect predissociation mechanism,<sup>26</sup> involving non-Born–Oppenheimer mixing with neighboring excited states, similar to what we previously found for HCl.<sup>5</sup> The derived relative detection sensitivity of HCl and DCI has recently been employed to determine the HCl and DCI product branching ratios in the reaction of Cl atoms with the selectively deuterated species  $(\text{CH}_3)_3\text{CD}$  and  $\text{CD}_3\text{CH}_2\text{CD}_3$  in order to compare the cross sections for abstraction of primary vs secondary or tertiary hydrogens from hydrocarbon reagents.<sup>19,27</sup>

Several studies of the one-photon VUV absorption and emission spectra of DCI have been reported.<sup>28–33</sup> Of greatest interest for REMPI detection of DCI is the observation and analysis of the  $E-X$  and  $F-X$  transitions by Douglas and Greening.<sup>32</sup> In contrast to the extensive work previously carried out on the REMPI spectrum of HCl,<sup>3–5,23–25,34–36</sup> little attention has been paid to the DCI isotopomer. Callaghan *et al.*<sup>23</sup> reported molecular constants for the (0,0) and (2,0) transitions to the  $E$  state and the (0,0), (1,0), and (2,0) transitions to the  $F$  state of DCI. Subsequently, Green *et al.*<sup>24</sup> reported transition wave numbers in a 2+1 REMPI spectrum for the rotational lines in the  $\text{D}^{35}\text{Cl}\ E\ ^1\Sigma^+ - X\ ^1\Sigma^+$  (0,0) band, but no study of REMPI intensity factors for any transition has been carried out for this molecule, to our knowledge. To complement our study of these intensity factors, we have measured accurate transition energies for several bands in the REMPI spectrum of DCI.

## II. APPARATUS

The experiments at Johns Hopkins University were carried out in a recently constructed time-of-flight mass spectrometer (TOFMS) which has been described in detail previously.<sup>18</sup> The ionization-extraction region and the flight tube are separately pumped by trapped oil diffusion pumps. DCI (Isotec, 99% atom D), or HCl (MG Industries, Inc., respectively) was bled into the ionization chamber through a variable leak valve (Granville Phillips) to pressures of  $\leq 2.5 \times 10^{-5}$  Torr. The resultant increase in pressure in the flight tube chamber was  $\leq 2 \times 10^{-7}$  Torr (ionization gauge readings). With this method of introducing the reagents, the rotational distributions follow a room-temperature Boltzmann distribution. The reagents were stored in a 0.25 l glass bulb, which could be evacuated with a diffusion pump.

The frequency-doubled output of an excimer laser pumped dye laser (Lambda Physik EMG101MSC/FL3002, operated at 10 Hz repetition rate) was employed for electronic excitation and ionization of the molecules. The UV radiation was separated from the visible output with dichroic optics and was focused into the ionization region of the

TOFMS with a 40 cm focal length fused silica lens. The UV pulse energies employed ranged from 0.3 to 1.5 mJ.

The TOFMS is of the Wiley–McLaren design,<sup>37</sup> with two acceleration regions. Following the ionization-extraction region, there are two sets of deflection electrodes for beam steering and an Einzel lens for beam collimation. The ions are detected at the end of the flight tube with dual micro-channel plates, whose output was monitored with either a gated integrator (SR250) or a digital oscilloscope (LeCroy 9360, 300 MHz analog bandwidth, maximum sampling rate 5 Gs/s). The parent and fragment ions ( $\text{DCI}^+$ ,  $\text{D}^+$ ,  $\text{Cl}^+$ ) were collected with equal efficiency, as was verified by the insensitivity of the ion signal intensities over a fairly wide range of Einzel lens focusing conditions. For measurement of the relative ion signals for different masses, several gated integrators simultaneously monitored the ion signals for these mass channels as a function of the UV laser wave number. For calibration of the laser wave number, scans of the ion signal were taken simultaneously with a neon optogalvanic spectrum and the transmission maxima of an étalon (free spectral range  $0.663\ \text{cm}^{-1}$  in the visible).

The apparatus at the University of Illinois at Chicago has been described previously<sup>4</sup> and is similar to the one used at Johns Hopkins. This apparatus was used to record the  $J$ -dependent anomalies in the  $F-X$  transitions and the correction factors for the  $F-X$  transitions in HCl and DCI. The UV laser energy was typically 0.5–1.0 mJ/pulse and was focused between the repeller and extractor plates with a 30 cm f.l. lens.

## III. RESULTS

### A. REMPI spectra and transition energies

Since accurate line positions for only the  $E-X$  (0,0) band have been reported previously in the REMPI spectrum of DCI, we have measured accurate transition energies for several bands of the  $F-X$  and  $V-X$  transitions. Table I presents our measured line positions for the  $\text{D}^{35}\text{Cl}\ F-X$  (0,0) and (1,0) bands. These line positions were fit to the expression

$$v(J', J'') = T_0 + T'_v(J') - F''_v(J''), \quad (1)$$

where

$$F_v(J) = B'_v J(J+1) - D'_v J^2(J+1)^2. \quad (2)$$

The resulting values of the band origin,  $T_0$ , and the rotational constants,  $B'_v$  and  $D'_v$ , are reported in Table II. In these fits,  $B''_0$  and  $D''_0$  were held fixed at the values ( $5.39226$  and  $1.4006 \times 10^{-6}\ \text{cm}^{-1}$ , respectively) obtained from accurate infrared measurements.<sup>38</sup> Consistent with analyses by other workers,<sup>24,29,32</sup> we allowed for the possibility of  $\Lambda$  doubling by fitting the  $e$  and  $f$  symmetry levels of the  $F\ ^1\Delta$  state separately.

As can be seen from Table II, our values for these parameters agree very well with the one-photon values reported by Douglas and Greening<sup>32</sup> for the  $F-X(0,0)$  band. The  $F-X(1,0)$  band was previously reported in the REMPI spectrum by Callaghan *et al.*,<sup>23</sup> and their constants agree with the

TABLE I. Measured transition wave numbers for the  $D^{35}\text{Cl } F^1\Delta-X^1\Sigma^+$  (0,0) and (1,0) bands.<sup>a</sup>

$J''$	$O(J)$	$P(J)$	$Q(J)$	$R(J)$	$S(J)$
(0,0) band					
0					82 940.94
1				82 929.91	82 961.10
2			82 908.27	82 939.61	82 980.78
3		82 875.94	82 906.86	82 948.35	83 000.02
4	82 832.88	82 863.89	82 905.30	82 956.90	83 018.69
5	82 810.00	82 851.47	82 902.83	82 964.92	83 036.94
6	82 786.54	82 838.46	82 900.25	82 972.60	83 054.96
7	82 762.83	82 825.00	82 897.23	82 979.69	83 072.02
8	82 738.84	82 810.99	82 893.70	82 986.03	83 088.87
9	82 714.12	82 796.81	82 889.32	82 992.33	
10	82 689.36	82 781.87	82 884.75		
(1,0) band					
0					84 768.26
1				84 757.40	84 806.77
2			84 735.76	84 766.25	84 825.08
3		84 703.32	84 733.85	84 774.51	84 842.52
4		84 690.53	84 731.09	84 781.79	
5		84 677.14	84 727.98	84 788.46	
6		84 663.05	84 723.88	84 794.57	
7		84 648.20	84 719.13	84 799.97	
8		84 632.84	84 713.76	84 804.49	
9			84 707.70		

<sup>a</sup>Estimated uncertainties in the transition wave numbers  $\pm 0.3 \text{ cm}^{-1}$ .

values reported in Table II. We believe the assignment of the (1,0) band is correct for several reasons. First, the rotational structure is consistent with  $\Omega'=2$ . In addition, this assignment leads to the derived vibrational spacing  $\Delta G_{1/2}=1828.0(4) \text{ cm}^{-1}$ . This value is quite close to the vibrational spacing in the  $\text{DCI}^+$  ion,  $\Delta G_{1/2}=1864.0 \text{ cm}^{-1}$  (Ref. 39). A similar vibrational spacing was previously noted for  $\text{HCl}(F)$  and  $\text{HCl}^+$  ( $\Delta G_{1/2}=2516.5$  and  $2568.62 \text{ cm}^{-1}$ , respectively),<sup>24</sup> as expected for these Rydberg states. Finally,

the only other nearby  $\Omega'=2$  state is expected to be the  $f^3\Delta_2(v'=1)$  level, which should lie  $\sim 800 \text{ cm}^{-1}$  lower in energy than  $F^1\Delta(v'=1)$ .<sup>24</sup> We also note that the REMPI intensity of the  $F-X$  (1,0) band was much weaker than for the  $F-X$  (0,0) band.

Douglas and Greening<sup>32</sup> report observations of the  $E-X$  (0,0) and (1,0) bands in one-photon VUV absorption spectroscopy of DCI. To complement the previous observations of the  $E-X$  (0,0) and (2,0) bands in the REMPI

TABLE II. Derived spectroscopic constants for  $D^{35}\text{Cl}$  excited electronic states.<sup>a</sup>

State	$v'$	$T_0$	$B'$	$D' \times 10^4$	$\Delta(35-37)^b$	Source <sup>c</sup>
$F^1\Delta$	0	82 909.8(3)	5.168(12)	1.6(10)		This work ( <i>e</i> )
		82 909.7(2)	5.166(9)	1.4(8)		This work ( <i>f</i> )
		82 909.5	5.164	1.4		Ref. 32 ( <i>e</i> )
	1		5.167	1.8		Ref. 32 ( <i>f</i> )
		84 737.8(3)	5.056(16)	1.0(17)		This work ( <i>e</i> )
		84 737.8(3)	5.068(17)	2.6(18)		This work ( <i>f</i> )
$V^1\Sigma^+$	15	84 299.4(2)	2.149(15)	-5.4(17)	7.3	This work
		84 298.2	2.166	-4.4	7.6	Ref. 32
	16	84 663.5(2)	2.387(15)	15.2(7)	7.5	This work
		84 663.9	2.405	18	7.4	Ref. 32
	17	84 952.6(3)	3.260(27)	31.4(48)	6.1	This work
		84 952.3	3.252	34	5.9	Ref. 32
	18	85 479.8(2)	2.229(20)	-45.8(28)	9.2	This work
		85 479.8	2.218	-46	9.4	Ref. 32
	19	85 843.2(2)	2.137(15)	-6.9(17)	9.7	This work
		85 842.8	2.143	-4.9	10.0	Ref. 32

<sup>a</sup>Quoted uncertainties are one standard deviation in units of the least significant quoted digit.<sup>b</sup> $D^{35}\text{Cl}-D^{37}\text{Cl}$  isotope splitting.<sup>c</sup>For the  $F^1\Delta$  state, *e* and *f* in parentheses denotes that the constants were determined by fits of lines terminating in excited *e* and *f* levels, respectively.

TABLE III. Measured transition wave numbers for the  $Q$ -branch lines of the  $D^{35}\text{Cl } V^1\Sigma^+ - X^1\Sigma^+ (v',0)$  bands.<sup>a</sup>

$J''$	$v'$				
	15	16	17	18	19
0	84 299.17	84 663.05	84 953.00	85 479.37	85 843.84
1	84 292.58	84 657.77	84 948.69	85 473.35	85 836.38
2	84 279.76	84 645.60	84 939.41	85 460.95	85 823.48
3	84 260.74	84 627.36	84 926.04	85 442.90	85 804.03
4	84 235.47	84 602.92	84 908.16	85 418.78	85 778.21
5	84 203.58	84 571.88	84 885.51	85 389.80	85 746.33
6	84 164.38	84 534.62	84 859.55	85 355.10	85 708.05
7	84 119.18	84 490.48	84 822.98	85 316.13	85 663.61
8	84 068.65	84 440.75		85 277.26	85 613.01
9	84 013.70	84 381.48			85 556.82

<sup>a</sup>Estimated uncertainties in the transition wave numbers  $\pm 0.3 \text{ cm}^{-1}$ .

spectrum,<sup>23,24</sup> we searched for the corresponding (1,0) band, whose origin is reported to be at  $85\,132 \text{ cm}^{-1}$  in the one-photon absorption spectrum.<sup>32</sup> No ion signals (parent or fragment) assignable to this band were found. We scanned from the origin of the  $E-X$  (0,0) band [ $83\,948.8 \text{ cm}^{-1}$  (Ref. 24)] to  $86\,000 \text{ cm}^{-1}$ . Over this wave number range, we observed only  $V^1\Sigma^+ - X^1\Sigma^+ (v',0)$  bands, with  $v' = 15-19$ . (The vibrational numbering was determined from analysis of the DCI emission and absorption spectra.<sup>32,33</sup>) The transition wave numbers for the  $Q$ -branches of these bands are reported in Table III. (Weak  $S$ - and  $O$ -branch transitions were also observed, but the transition wave numbers of these lines are not reported here.) The derived origins and rotational constants for the  $V-X$  bands are given in Table II. As can be seen from this table, there is very good agreement of our derived constants with those reported by Douglas and Greening.<sup>32</sup> From our signal-to-noise ratio, the REMPI intensity of the unobserved  $E-X$  (1,0) band must be at least an order of magnitude smaller than the intensities of the adjacent observed  $V-X$  bands.

## B. Intensity factors in the $E-X$ (0,0) band

Previous REMPI experiments have shown that ionization of HCl through  $\Omega' = 0^+$  states leads to extensive fragmentation, yielding both parent  $\text{HCl}^+$  and fragment  $\text{Cl}^+$  and  $\text{H}^+$  ions.<sup>3,24,25</sup> In a similar fashion, we find that fragmentation also occurs for resonant ionization of DCI through its  $E^1\Sigma^+$  state. Figure 1 shows the REMPI spectrum of the  $E-X$  (0,0) band, with detection of the  $\text{DCI}^+$ ,  $\text{Cl}^+$ , and  $\text{D}^+$  ions. We see that the relative intensities of the  $Q$ -branch lines are similar in the three ion channels. Beyond  $J'' = 9$ , the  $Q$ -branch is obscured by the  $V-X$  (14,0) band, which occurs slightly to the red of the  $E-X$  (0,0) band.

In Fig. 1, the  $\text{DCI}^+$  and  $\text{Cl}^+$  ion signals are comparable in intensity, while those for  $\text{D}^+$  ions are somewhat smaller. We also notice that lines of both the  $\text{D}^{35}\text{Cl}$  and  $\text{D}^{37}\text{Cl}$  isotopomers are observed in the  $\text{DCI}^+$  and  $\text{D}^+$  ion channels ( $m/e = 37$  and  $2$ , respectively). For  $m/e = 37$ , these arise from the parent ion through ionization of  $\text{D}^{35}\text{Cl}$  and from the  $\text{Cl}^+$  fragment ion produced from  $\text{D}^{37}\text{Cl}$ . Unfortunately, this leads

to the overlapping of several  $\text{D}^{35}\text{Cl}$  and  $\text{D}^{37}\text{Cl}$  lines; in particular, the  $Q(1)$  line of  $\text{D}^{35}\text{Cl}$  is overlapped by the  $Q(0)$  line of  $\text{D}^{37}\text{Cl}$ .

We have measured the relative signals for detection of  $\text{DCI}^+$ ,  $\text{Cl}^+$ , and  $\text{D}^+$  ions for resonant ionization through the  $Q$ -branch lines of  $\text{D}^{35}\text{Cl}$  at several UV laser pulse energies. In the absence of saturation effects in the two-photon excitation step, alignment in the ground state, and dissociation, the theoretical REMPI intensities for  $\text{DCI}^+$  are given by

$$I = C[P(v'', J'') / (2J'' + 1)]q(v', v'')S(J', J''). \quad (3)$$

In Eq. (3),  $P(v'', J'')$  is the population of molecules in the  $v'', J''$  level,  $q(v', v'')$  is the Franck-Condon factor,

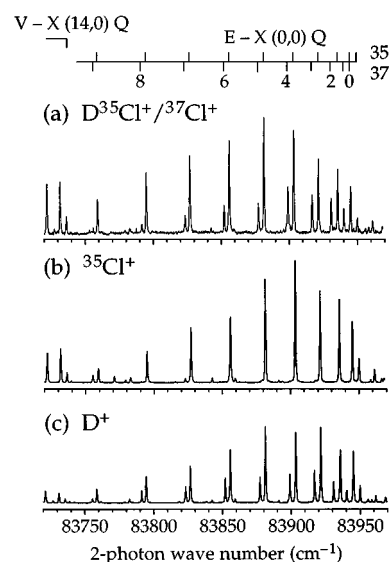


FIG. 1. REMPI spectrum for a thermal DCI sample showing the  $E^1\Sigma^+ - X^1\Sigma^+ (0,0)$  band detected in the (a)  $m/e = 37$  ( $\text{D}^{35}\text{Cl}^+$  and  $\text{D}^{37}\text{Cl}^+$ ), (b)  $m/e = 35$  ( $\text{Cl}^+$ ), and (c)  $m/e = 2$  ( $\text{D}^+$ ) ion channels. The ordinates in all three panels are plotted with the same scaling. The UV laser pulse energy was 1 mJ. The  $Q$ -branch lines of the  $\text{D}^{35}\text{Cl}$  and  $\text{D}^{37}\text{Cl}$  isotopomers are indicated. The  $Q$ -branch of the  $V-X$  (14,0) bandhead of  $\text{D}^{35}\text{Cl}$  is also marked.

$S(J', J'')$  is the two-photon rotational line strength factor,<sup>40</sup> and  $C$  is a  $v', J'$ -dependent apparatus constant which is proportional to the square of the laser intensity, the absorption cross section, and the quantum yield. The quantum numbers  $v''$  and  $J''$  denote the vibrational level and total angular momentum in the ground state, while  $v'$  and  $J'$  are the corresponding quantities in the resonantly excited state.

The line strength factors for the  $Q$ -branch of a  $\Sigma-\Sigma$  transition can be written as

$$S_Q(J', J'') = (2J'' + 1) \left[ 1 + (\mu_s^2 / \mu_i^2) \times \frac{J''(2J'' + 1)}{5(2J'' - 1)(2J'' + 3)} \right], \quad (4)$$

where  $(\mu_s^2 / \mu_i^2)$  is a ratio of transition dipole moments, in the notation of Kummel, Sitz, and Zare.<sup>41</sup> The factor  $(\mu_s^2 / \mu_i^2)$  may be estimated by comparing the ratio of the intensities of the  $Q(2)$  and  $O(2)$  lines. For an  $O$ -branch transition, the line strength factor equals

$$S_O(J', J'') = (\mu_s^2 / \mu_i^2) \frac{3J''(J'' - 1)}{10(2J'' - 1)(2J'' + 1)}. \quad (5)$$

Unfortunately, the  $O(2)$  line of  $D^{35}\text{Cl}$  [at  $83\,916.5\text{ cm}^{-1}$  (Ref. 24)] in the  $m/e=37$  channel is obscured by the  $Q(3)$  line of  $D^{37}\text{Cl}$  (see Fig. 1). Instead, we have compared the intensities of the  $Q(2)$  and  $O(2)$  lines for  $^{35}\text{Cl}^+$  detection. This ratio equals  $61 \pm 9$  and  $41 \pm 6$  for UV energies of 0.5 and 1 mJ, and from Eqs. (4) and (5) we obtain  $(\mu_s^2 / \mu_i^2) = 0.42$  and 0.64, respectively. These values are similar to the ratio previously reported by Spiglanin *et al.*<sup>3</sup> for the  $\text{HCl } E-X(0,0)$  band [ $(\mu_s^2 / \mu_i^2) = 0.38$ ]. In fact, because the second term in the square brackets in Eq. (4) is small compared to unity, the actual contribution of this term to  $S_Q(J', J'')$  is small ( $<5\%$ ). We have used the value  $(\mu_s^2 / \mu_i^2) = 0.42$  for the calculation of these line strength factors.

Since the DCI sample in our experiment has a room-temperature rotational state distribution, we may use Eq. (3) to calculate the apparatus constant  $C$  for REMPI detection of either parent or fragment ions through the  $Q$ -branch lines. Figure 2(a) presents the measured relative apparatus constant  $C$  for REMPI detection of  $D^{35}\text{Cl}^+$  using the  $Q$ -branch of the  $E-X(0,0)$  band. In Fig. 2(b) are plotted the ratios of the ion signals for the detection of the fragment ions ( $\text{Cl}^+$  or  $\text{D}^+$ ) vs the parent  $\text{DCI}^+$  ion signal for these two laser pulse energies. For both the  $\text{DCI}^+$  and  $\text{D}^+$  ion channels, we dealt with the overlap of the  $Q(1)$  line of  $D^{35}\text{Cl}$  by the  $Q(0)$  line of  $D^{37}\text{Cl}$  by subtracting an estimated contribution from the latter based on the ratio of the  $D^{35}\text{Cl}$  and  $D^{37}\text{Cl}$  signals observed for higher  $J$  levels.

We normally expect the ion signals to scale as the square of the laser pulse energy, if the two-photon excitation step is not saturated and the ionization step is saturated. To facilitate comparison of the apparatus factor at 0.5 and 1 mJ, we multiplied the signals at the lower laser energy by 4. We see in Fig. 2(a) that the energy-scaled factors  $C$  for the two pulse

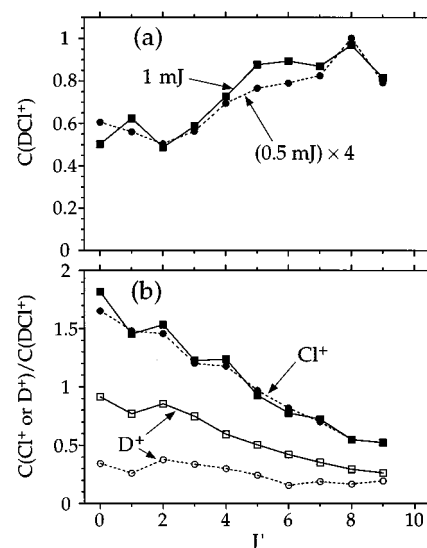


FIG. 2. The apparatus constants  $C$  [defined in Eq. (3)] for REMPI detection of the  $Q$ -branch lines of the  $D^{35}\text{Cl } E-X(0,0)$  band, with 0.5 (circles and dotted lines) and 1 mJ (squares and solid lines) UV laser pulse energies. (a) presents the empirical correction factors  $C$ . The values for 0.5 mJ pulse energy were multiplied by 4 (to correct for an assumed quadratic energy dependence) and normalized to unity for  $J'=8$ . (b) presents ratios of the  $C$  factors for detection of  $\text{Cl}^+$  vs  $\text{DCI}^+$  (solid symbols) and for detection of  $\text{D}^+$  vs  $\text{DCI}^+$  (open symbols) at 0.5 and 1 mJ pulse energy.

energies are almost superimposable, indicating that the parent ion signals do scale with the square of the laser pulse energy under our conditions.

Figure 2(b) shows that ion fragmentation occurs much more readily for low- $J$  levels than for high- $J$  levels of DCI. Indeed, for  $J \leq 4$ , the fragment  $\text{Cl}^+$  signal is greater than that for the parent ion. We also see that the ratio of the  $\text{Cl}^+$  to  $\text{DCI}^+$  signals is independent of the laser pulse energy under the conditions investigated. In contrast, the fragment  $\text{D}^+$  signals are significantly smaller than the corresponding parent ion signals; moreover, the  $\text{D}^+$  signal is considerably reduced at the lower laser pulse energy.

### C. Rotational intensity anomalies in the HCl and DCI REMPI signals

In previous studies with room-temperature samples,<sup>3-5</sup> it was found that the intensities of the  $\text{HCl } F-X$  and  $E-X$  transitions deviate from the values expected for a Boltzmann population, suggesting the existence of predissociative loss mechanisms. We report here similar behavior for the  $F-X(0,0)$ ,  $F-X(1,0)$ , and  $E-X(0,0)$  bands of DCI, displayed as “Boltzmann plots” in the top panels of Figs. 3-5, respectively. For this isotopomer, the intensity loss due to predissociation increases monotonically for both bands of the  $F-X$  transition, while for the  $E-X(0,0)$  band the intensity loss is greatest for small  $J$ . Empirical correction factors were calculated by equating the experimental parent ion signals with the Boltzmann populations at  $J''=3$  for the  $F-X$  bands and at  $J''=8$  for the  $E-X$  band. These results are listed for the  $F-X$  bands in Tables IV and V. In determining the ion intensities for these bands, the laser energy was kept below 0.5

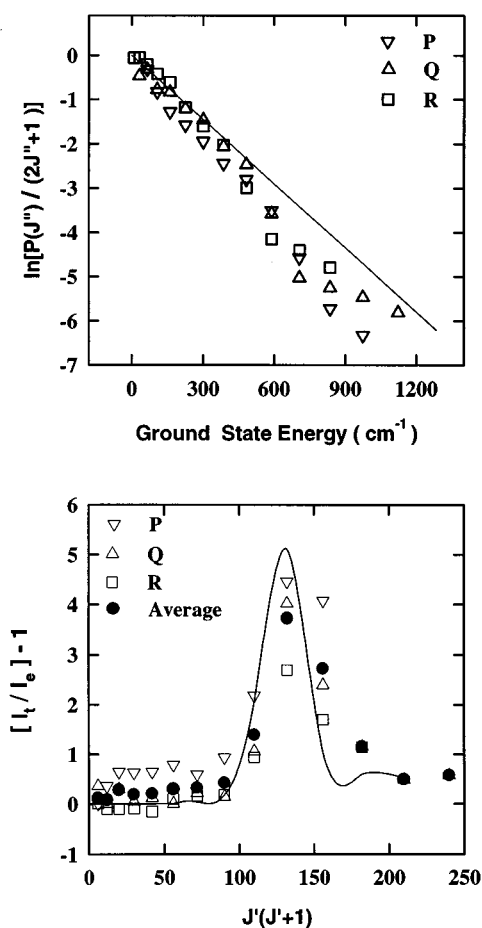


FIG. 3. The DCI  $F^1\Delta-X^1\Sigma^+(0,0)$  transition. (Top panel) Boltzmann plot of the apparent rotational populations (obtained by dividing the experimental parent ion signal by the rotational line strength  $S$ ). The line indicates the population for a 300 K thermal distribution, divided by the  $(2J''+1)$  degeneracy. (Bottom panel) Plot of the intensity anomaly vs  $J'(J'+1)$ . The filled circles are the average of the  $P$ -,  $Q$ -, and  $R$ -branches. The curve is a least squares fit, calculated according to the model described in the text.

mJ/pulse; at higher energy, saturation begins to set in, and the intensity on the  $R(1)$  line starts to become depressed relative to the intensities of the other lines.

Liyanage *et al.*<sup>5</sup> presented previously a “Boltzmann plot” for the HCl  $F-X(0,0)$  transition. Empirical correction factors  $C$  for the HCl  $F-X(0,0)$  and  $(1,0)$  transitions are listed in Tables VI and VII, respectively. The  $C$  factors were normalized in these tables by equating the experimental parent ion signals with the Boltzmann populations at  $J''=12$  and 5 for the  $(0,0)$  and  $(1,0)$  bands, respectively. For comparison with the corresponding DCI transition, we present in the top panel of Fig. 6 a “Boltzmann plot” for the HCl  $E-X(0,0)$  transition. As noted previously,<sup>3</sup> we see that the intensity loss increases with increasing rotational energy.

#### D. Comparison of HCl and DCI REMPI sensitivities

The most convenient transitions with which to compare the relative concentrations of HCl and DCI are their respective  $F-X(0,0)$  bands since the origins of these bands are

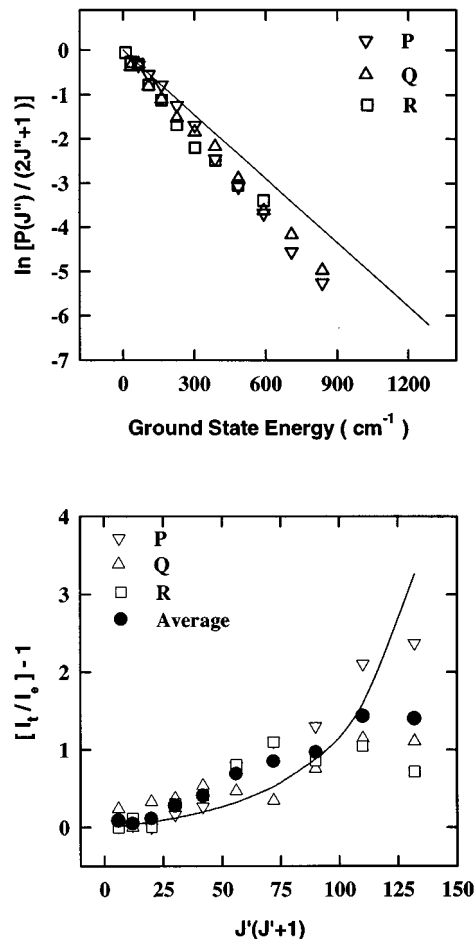


FIG. 4. Same as Fig. 3, for the DCI  $F^1\Delta-X^1\Sigma^+(1,0)$  transition.

only  $37\text{ cm}^{-1}$  apart, and excitation through the  $F$  state is observed to lead to exclusive formation of parent ions. We have compared the relative intensities, for excitation through the  $R(1)$  lines, of the respective bands of these isotopomers. In this study, HCl or DCI was bled in separate runs through a leak valve into the ionization-extraction region of the TOFMS. The HCl and DCI pressures were determined with an ionization gauge, which was assumed to have the same calibration factor for both isotopomers. Between these runs, the glass gas-handling manifold was evacuated with a diffusion pump, and the walls were passivated.

The measured  $R(1)$  ion signal intensities were measured and converted into apparatus detection factors  $C$  [see Eq. (3)] by taking into account the fraction of the total concentration of each isotopomer in the  $J''=1$  rotational level. We plot in Fig. 7(a) the relative values of the factor  $C$  for  $\text{H}^{35}\text{Cl}^+$  and  $\text{D}^{35}\text{Cl}^+$  detection as a function of the square of the UV laser pulse energy, for equal partial pressures of HCl and DCI. We see that the  $\text{H}^{35}\text{Cl}^+$  ion signal from ionization of HCl scales as the power squared up to 1.3 mJ, the highest pulse energy investigated. In contrast, the  $\text{D}^{35}\text{Cl}^+$  signal from ionization of DCI demonstrates the onset of saturation, as noted in the previous section, and falls below this scaling law at pulse energies slightly less than 1 mJ. Figure 7(b)

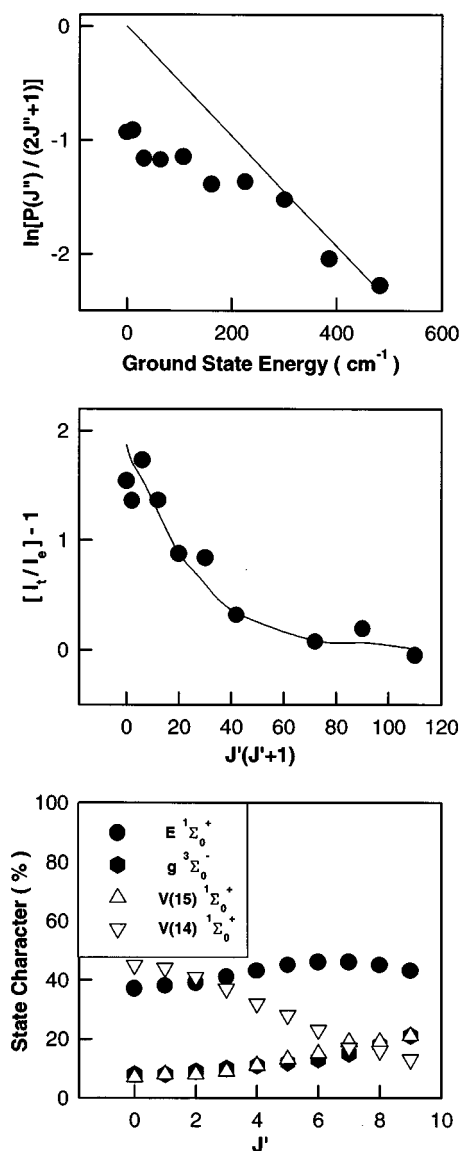


FIG. 5. The DCI  $E\ 1\Sigma^+ - X\ 1\Sigma^+$  (0,0) transition. (Top panel) Boltzmann plot of the apparent rotational populations (obtained by dividing the experimental parent ion signal by the rotational line strength  $S$ ). The line indicates the population for a 300 K thermal distribution, divided by the  $(2J''+1)$  degeneracy. (Middle panel) Plot of the intensity anomaly for the  $Q$ -branch vs  $J'(J'+1)$ ; the curve is a least squares fit, calculated according to the model described in the text. (Bottom panel) Percent contributions of the  $E\ 1\Sigma^+$ ,  $g\ 3\Sigma^-$ , and  $V(15)\ 1\Sigma^+$  and  $V(14)\ 1\Sigma^+$  basis functions to the  $E\ 1\Sigma^+$  ( $v'=0$ ) eigenfunctions.

presents a plot of the ratio of the detection factors  $C$  for DCI vs HCl as a function of the UV laser pulse energy. We see that the detection sensitivity for DCI is significantly greater than for HCl. In addition, because of the saturation of the DCI<sup>+</sup> ion signal, noted in Fig. 7(a), this ratio displays a significant dependence on the laser pulse energy above 0.8 mJ.

In practice, it is often convenient to raise the laser probe energy into the partially saturated regime [ $>0.8$  mJ in Fig. 7(b)] in order to maximize the detected product signal. Indeed, this was done in our recent studies of the DCI vs HCl

TABLE IV. Correction factors<sup>a</sup> for the  $D^{35}Cl\ F\ 1\Delta - X\ 1\Sigma^+$  (0,0) band.

$J''$	$C(P)$	$C(Q)$	$C(R)$
0			
1			0.990
2		0.995	1.112
3	0.994	0.772	1.107
4	0.735	0.949	1.099
5	0.606	0.888	1.173
6	0.615	0.989	0.908
7	0.607	0.817	0.858
8	0.560	0.870	0.845
9	0.627	0.485	0.516
10	0.517	0.199	0.271
11	0.314	0.294	0.371
12	0.183	0.464	0.466
13	0.197	0.671	
14		0.635	
15		0.946	

<sup>a</sup>The factor  $C$ , defined in Eq. (3).

TABLE V. Correction factors<sup>a</sup> for the  $D^{35}Cl\ F\ 1\Delta - X\ 1\Sigma^+$  (1,0) band.

$J''$	$C(P)$	$C(Q)$	$C(R)$
0			
1			1.000
2		0.808	0.900
3	0.986	0.999	0.996
4	0.971	0.752	0.779
5	0.999	0.728	0.710
6	0.859	0.651	0.554
7	0.791	0.681	0.476
8	0.557	0.742	0.539
9	0.475	0.569	0.489
10	0.435	0.466	0.583
11	0.322	0.474	
12	0.230	0.395	

<sup>a</sup>The factor  $C$ , defined in Eq. (3).

TABLE VI. Correction factors<sup>a</sup> for the  $H^{35}Cl\ F\ 1\Delta - X\ 1\Sigma^+$  (0,0) band.

$J''$	$C(P)$	$C(Q)$	$C(R)$
0			
1			0.573
2		0.812	...
3	0.778	0.623	0.500
4	0.577	0.444	0.419
5	0.405	0.365	0.385
6	0.373	0.334	0.391
7	0.300	0.313	0.392
8	0.319	0.324	0.573
9	0.347	0.280	...
10		0.664	0.911
11		1.019	1.055
12		1.020	1.000

<sup>a</sup>The factor  $C$ , defined in Eq. (3).

TABLE VII. Correction factors<sup>a</sup> for the H<sup>35</sup>Cl  $F^1\Delta-X^1\Sigma^+(1,0)$  band.

$J''$	$C(P)$	$C(Q)$	$C(R)$
0			
1			0.893
2		0.282	0.774
3	0.762	0.687	0.999
4	0.908	0.703	0.999
5	0.861	1.000	0.857
6	1.000	0.805	0.608
7	0.999	0.637	0.459
8	0.585	0.689	0.271
9	0.477		

<sup>a</sup>The factor  $C$ , defined in Eq. (3).

product branching in the Cl+(CH<sub>3</sub>)<sub>3</sub>CD and CD<sub>3</sub>CH<sub>2</sub>CD<sub>3</sub> reactions.<sup>19,27</sup> Under these circumstances, it is important to ensure that the calibration of the relative detection sensitivities is carried out under similar conditions.

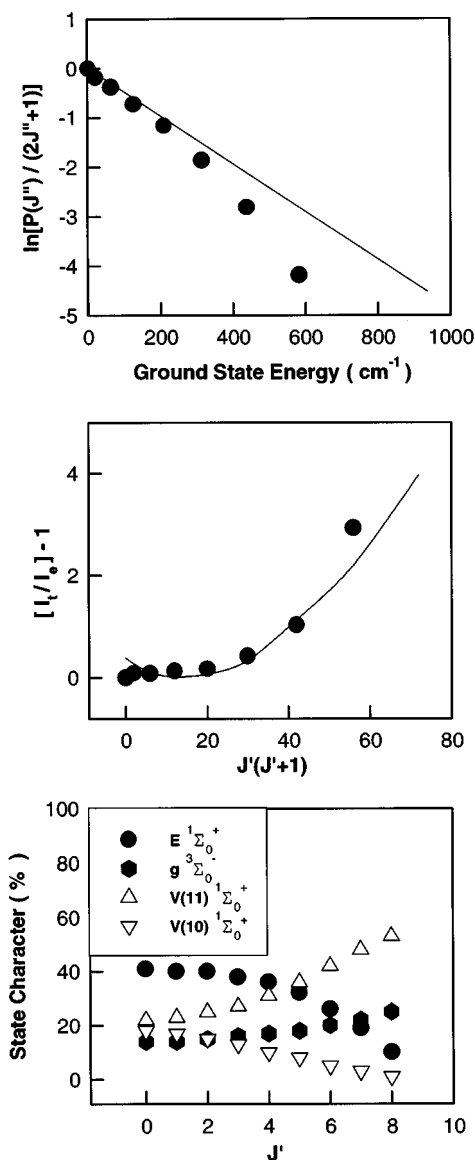


FIG. 6. Same as Fig. 5, for the HCl  $E^1\Sigma^+-X^1\Sigma^+(0,0)$  transition.

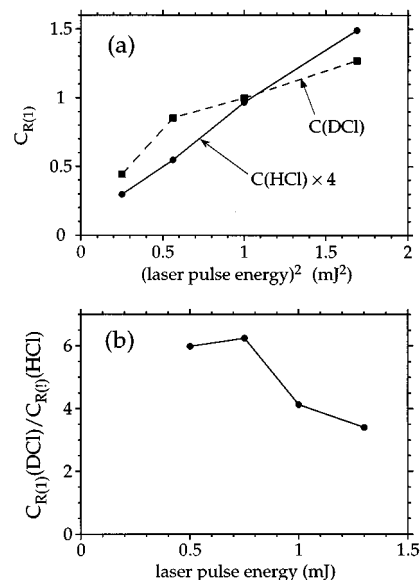
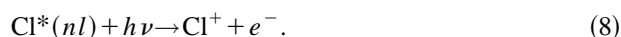


FIG. 7. (a) Apparatus constants  $C$  [see Eq. (3)] for REMPI detection through the  $F-X(0,0)R(1)$  lines of H<sup>35</sup>Cl (circles connected by solid lines) and D<sup>35</sup>Cl (squares connected by dashed lines), plotted as a function of the square of the UV laser pulse energy. For both isotopomers,  $C$  was normalized to unity for D<sup>35</sup>Cl at 1 mJ pulse energy. The values of  $C$  for H<sup>35</sup>Cl have been multiplied by a factor of 4. (b) Plot of the ratio of the  $C$  constants for D<sup>35</sup>Cl vs H<sup>35</sup>Cl as a function of the UV laser pulse energy.

#### IV. DISCUSSION

We have found for the  $E$  state of DCI that the ratio of fragment (both Cl<sup>+</sup> and D<sup>+</sup>) to parent ion signals decreases significantly with increasing  $J'$ . From the point of view of detection of DCI in a reaction mixture, the observation of a fragment ion, particularly D<sup>+</sup>, in REMPI detection may be advantageous. For example, a strong Cl<sup>+</sup> signal from non-resonant ionization of a reagent, for example Cl<sub>2</sub>, could obscure the observation of the parent ion, whereas detection of D<sup>+</sup> might be cleaner because of its short flight time.

The formation of fragment ions in the wavelength range we have probed requires the absorption of at least four photons. Green and Wallace<sup>25</sup> have discussed extensively the processes which could lead to the formation of fragment ions in the multiphoton ionization of HCl. They concluded that for  $\Omega'=0^+$  states above the  $V^1\Sigma^+(v'=3)$  level, the most likely process involves an indirect dissociation of three-photon excited HCl to form ground and electronically excited atoms, which are then subsequently ionized by the absorption of one more photon,



The excited atomic states, in particular H<sup>\*</sup>( $n=2$ ) and Cl<sup>\*</sup>( $2D^0, 2S^0$ ), have been observed by photoelectron

spectroscopy.<sup>35</sup> At our experimental energies the only accessible excited states are  $H(n=2)$  and those derived from  $Cl(3p^4 4s)$  and  $Cl(3p^4 4p)$ . Fluorescence measurements have shown that the  $H(n=2)$  product is a minor component.<sup>42,43</sup>

The intensity anomalies in the REMPI spectra of HCl and DCI can be understood by considering the competition between the rates of predissociation and photoionization of the excited states.<sup>5</sup> We start by expressing the two-photon excited state eigenfunction  $|\Psi\rangle$  as a linear combination of interacting zero-order states  $|s\rangle$ ,

$$|\Psi\rangle = \sum_s c_s |s\rangle. \quad (9)$$

The predissociation rate of  $|\Psi\rangle$  is proportional to the squared matrix element

$$|\langle\Psi|\mathcal{H}|\chi\rangle|^2 \propto \sum_s c_s^2 k_s + 2 \sum_{s,s'} p_{ss'} c_s c_{s'} (k_s k_{s'})^{1/2}, \quad (10)$$

where  $\mathcal{H}$  is the operator that couples  $|\Psi\rangle$  to the continuum state  $|\chi\rangle$ ,  $k_s$  is the predissociation rate of  $|s\rangle$ , and  $p_{ss'}$  is a phase factor equal to  $\pm 1$ . In addition to predissociating,  $|s\rangle$  can also absorb another photon and ionize at a rate  $\Gamma_s$ . We define the ratio of dissociation to ionization rates as

$$g_s = k_s / \Gamma_s. \quad (11)$$

The intensity anomaly (i.e., the missing signal due to the predissociation channel) can then be written as

$$I_t / I_e - 1 = \sum_s c_s^2 g_s + 2 \sum_{s,s'} p_{ss'} c_s c_{s'} (g_s g_{s'})^{1/2}, \quad (12)$$

where  $I_t$  is the signal that would be obtained if the state were unperturbed, and  $I_e$  is the observed (perturbed) signal. [Note that if  $g_s = 0$  (no predissociation), then  $I_t = I_e$ .]

We illustrate these results for the simple case of two interacting states,

$$|\Psi\rangle = c_1 |\Psi_0\rangle + c_2 |d\rangle, \quad (13)$$

where  $|\Psi_0\rangle$  is a discrete state and  $|d\rangle$  is a dissociative perturbing state. The intensity anomaly is given in this case by

$$I_t / I_e - 1 = c_1^2 g_1 + c_2^2 g_2 + 2 p_{12} c_1 c_2 (g_1 g_2)^{1/2}. \quad (14)$$

Setting  $g_1 = 0$  for  $|\Psi_0\rangle$  gives

$$I_t / I_e - 1 = c_2^2 g_2. \quad (15)$$

Using first-order perturbation theory, we obtain for  $c_1$  and  $c_2$

$$c_1 = [1 + (\mathcal{H}_{12} / \Delta E)^2]^{-1/2} \quad (16)$$

and

$$c_2 = c_1 \mathcal{H}_{12} / \Delta E, \quad (17)$$

where  $\mathcal{H}_{12}$  is a matrix element of the electronic Hamiltonian connecting states 1 and 2,  $\Delta E$  is the energy splitting of the unperturbed states, and  $\mathcal{H}_{12} \ll \Delta E$ . In this limit, we obtain

$$I_t / I_e - 1 = (\mathcal{H}_{12} / \Delta E)^2 g_2. \quad (18)$$

As discussed previously in detail for HCl,<sup>5</sup> the  $F^1\Delta$  state is coupled by non-Born–Oppenheimer interactions with predissociating excited states, which lead to a loss of ion intensity. For the  $F^1\Delta$  state, this mixing is dominated by the  $L$ -uncoupling operator, which mixes  $\Delta$  and  $\Pi$  states,

$$\begin{aligned} \langle F^1\Delta_2, v' | -B(J_+ L_- + J_- L_+) | C^1\Pi_1, v'' \rangle \\ = -B_{v', v''} b [J(J+1) - 2]^{1/2}, \end{aligned} \quad (19)$$

whereas, for the  $E^1\Sigma^+$  state, it is governed predominantly by an electrostatic interaction which mixes  $E^1\Sigma^+$  with  $V^1\Sigma^+$ . In addition, for the  $F^1\Delta$  state, we must also consider spin–orbit coupling to the  $f^3\Delta_2$  state, which in turn is coupled to the  $b^3\Pi_1$  state by an expression equivalent to Eq. (19). In Eq. (19)  $B_{v', v''}$  is a rotational overlap integral,

$$B_{v', v''} = \langle v' | \hbar^2 / 2\mu R^2 | v'' \rangle, \quad (20)$$

and  $b$  is proportional to an  $l$ -mixing coefficient,

$$b = 2^{1/2} C_{4p}. \quad (21)$$

The  $(X^2\Pi)4p\pi$  Rydberg states (e.g.,  $F^1\Delta$  and  $f^3\Delta$ ) can interact with  $(X^2\Pi)4s\sigma$  states (e.g.,  $C^1\Pi$  and  $b^3\Pi$ ) only if  $4s\sigma$  has some  $4p\sigma$  character, with a mixing coefficient  $C_{4p}$ .<sup>26</sup>

The  $e^3\Sigma^+$  state plays only a minor role in the perturbation of the  $F$  and  $E$  states because it does not couple directly to either of them. (The matrix elements for the spin–orbit, rotation, and electrostatic terms in the Hamiltonian coupling these states are all zero.<sup>26</sup>) Moreover, the  $e$  state is too remote energetically from the  $F$  state to interact with it significantly.<sup>25</sup> Indirect coupling via spin–orbit mixing with the  $d^3\Pi$  state was included in the calculation but had only a minor effect.

### A. $F-X(0,0)$ transition of DCI

The  $F^1\Delta(v'=0)$  state of DCI ( $\nu_{00} = 82\,883\text{ cm}^{-1}$ ) is perturbed by the  $b^3\Pi_1(v'=4)$  state ( $\nu_{00} = 82\,750 \pm 300\text{ cm}^{-1}$ ) via the  $L$ -uncoupling operator. Before evaluating the strength of this interaction, we must first take into account the spin–orbit mixing of  $F^1\Delta$  with  $f^3\Delta_2$  and  $C^1\Pi$  with  $b^3\Pi_1$ . The spin–orbit mixed states are given by

$$\begin{aligned} |F^1\Delta_2(v'=0)\rangle' &= a_1 |F^1\Delta_2(v'=0)\rangle^0 \\ &+ a_2 |f^3\Delta_2(v'=0)\rangle^0, \end{aligned} \quad (22)$$

and

$$\begin{aligned} |b^3\Pi_1(v'=4)\rangle' &= b_1 |C^1\Pi_1(v'=3)\rangle^0 \\ &+ b_2 |b^3\Pi_1(v'=4)\rangle^0, \end{aligned} \quad (23)$$

where  $a_1$  and  $a_2$  are estimated<sup>44</sup> to be 0.88 and 0.47, and  $b_1$  and  $b_2$  are estimated to be 0.8 and 0.6. In Eqs. (22) and (23), the primes refer to spin–orbit mixed states and the superscripts 0 refer to zero-order states. Identifying  $|F^1\Delta_2(v'=0)\rangle'$  with  $|\Psi_0\rangle$  and  $|b^3\Pi_1(v'=4)\rangle'$  with  $|d\rangle$  in Eq. (13), we obtain

$$\begin{aligned} \mathcal{H}_{12} &= a_1 b_1^0 \langle F^1\Delta_2(v'=0) | -B(J_+ L_- + J_- L_+) | \\ &\times C^1\Pi_1(v'=3) \rangle^0 \\ &= -2^{1/2} C_{4p} a_1 b_1 B_{0,3} [J(J+1) - 2]^{1/2}, \end{aligned} \quad (24)$$

where  $B_{0,3}$  is estimated from Eq. (20) to equal  $1.23 \text{ cm}^{-1}$ . The triplet part of the  $|F^1\Delta\rangle'$  wave function contributes very little to  $\mathcal{H}_{12}$  because  $B_{0,4}$  is small. Inserting Eq. (24) into Eq. (18), we obtain a reasonable fit of the intensity anomaly with parameters  $C_{4p}^2 g \approx 5.4$  for  $C^1\Pi(v'=3)$ ,  $C_{4p}^2 g \approx 13$ ,  $B=4.7 \text{ cm}^{-1}$ , and a term energy of  $82\,990 \text{ cm}^{-1}$  for  $b^3\Pi_1(v'=4)$ , and  $p=-1$ , as shown in the bottom panel of Fig. 3. [It is important to note that, as seen from Eq. (15), we cannot obtain  $C_{4p}$  and  $g$  independently.]

Previously, we obtained  $C_{4p}^2 g \approx 60$  for the  $C^1\Pi(v'=2)$  state of HCl.<sup>5</sup> Assuming that the ionization rates and mixing coefficients for HCl and DCI are approximately equal,<sup>45</sup> the much smaller value of  $C_{4p}^2 g$  obtained for DCI implies a correspondingly smaller predissociation rate for this molecule. This conclusion is qualitatively consistent with the larger ion production efficiency of DCI shown in Fig. 7. It is also consistent with the one-photon spectra of Tilford *et al.*,<sup>29</sup> in which the  $C^1\Pi(v'=3) \leftarrow X$  transition of DCI is rotationally resolved, whereas the  $C^1\Pi(v'=2) \leftarrow X$  transition of HCl is not.

### B. $F-X(1,0)$ transition of DCI

The analysis of the  $F^1\Delta(v'=1) \leftarrow X^1\Sigma^+(v''=0)$  transition is similar to the corresponding (0,0) band, except that here the interaction is between the  $F(v'=1, \nu_{00}=84\,735 \text{ cm}^{-1})$  and  $C(v'=4, \nu_{00}=84\,941 \text{ cm}^{-1})$  spin-orbit mixed states. Here we identify  $|\Psi_0\rangle$  with

$$|F^1\Delta_2(v'=1)\rangle' = a_1|F^1\Delta_2(v'=1)\rangle^0 + a_2|f^3\Delta_2(v'=1)\rangle^0, \quad (25)$$

and  $|d\rangle$  with

$$|C^1\Pi_1(v'=4)\rangle' = b_1|C^1\Pi_1(v'=4)\rangle^0 + b_2|b^3\Pi_1(v'=5)\rangle^0, \quad (26)$$

in which  $a_1 \approx 0.88$ ,  $a_2 \approx 0.45$ ,  $b_1 \approx 0.8$ , and  $b_2 \approx 0.6$ . The best fit to the data was obtained for  $C_{4p}^2 g_2 \approx 50$ , where for simplicity we assumed that this quantity is the same for both the  $b$  and  $C$  states. As seen in the bottom panel of Fig. 4, the fit was not as good in this case. A possible cause for this poorer fit is that we assumed a common value of  $g_2$  for all perturbing states, whereas in fact the ratio of ionization to dissociation rates is probably state-dependent.

### C. $F-X$ transitions of HCl

The  $F^1\Delta(v'=0) \leftarrow X^1\Sigma^+(v''=0)$  transition in HCl has already been analyzed in Ref. 5. The (1,0) transition can be similarly analyzed in terms of an interaction between  $F^1\Delta(v'=1, \nu_{00}=85\,363 \text{ cm}^{-1})$  and  $b^3\Pi_1(v'=4, \nu_{00}=85\,162 \pm 300 \text{ cm}^{-1})$ . In this case,  $\mathcal{H}_{12}$  has non-negligible contributions from both singlet and triplet states. A reasonable fit was obtained for  $C_{4p}^2 g_2 \approx 6.3$ , as shown in Fig. 8. The smaller value of this quantity for HCl indicates

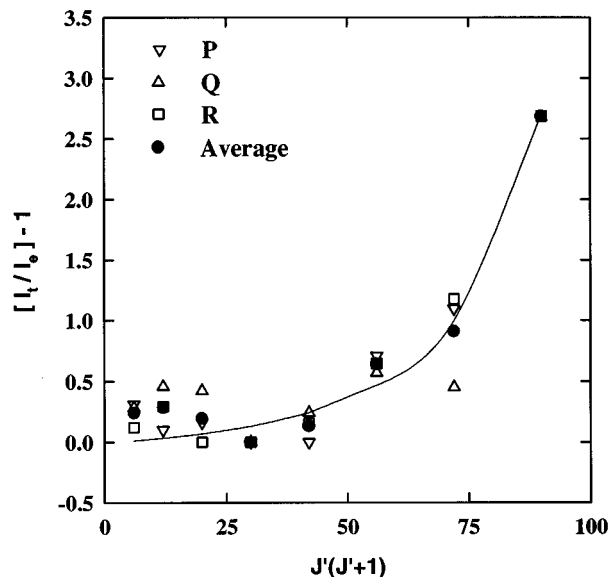


FIG. 8. Intensity anomaly for the HCl  $F^1\Delta-X^1\Sigma^+(1,0)$  transition. The filled circles are the average of the  $P$ -,  $Q$ -, and  $R$ -branches. The curve is a least squares fit, calculated according to the model described in the text.

that HCl( $F^1\Delta_2, v'=1$ ) dissociates more slowly than DCI( $F^1\Delta_2, v'=1$ ). (This is opposite the usual isotope dependence and is further evidence of a special predissociation mechanism.)

### D. $E-X(0,0)$ transitions of DCI and HCl

As shown in the middle panels of Figs. 5 and 6 for DCI and HCl, respectively, the  $J'$  dependence of the  $E^1\Sigma^+(v'=0) \leftarrow X^1\Sigma^+(v''=0)$  intensity anomaly differs qualitatively from that of the  $F-X$  transitions. For HCl the intensity anomaly of the  $E-X$  transition increases monotonically for  $J' > 4$ , while for DCI it decreases smoothly with increasing  $J'$ . The  $E$  state is perturbed mainly by electrostatic interaction with different vibrational levels of the  $V^1\Sigma^+$  state and spin-orbit mixing with the  $g^3\Sigma_0^-$  state. Since the  $V$  state is also mixed with other  $\Omega=0^+$  states, a complete deperturbation requires diagonalization of the Hamiltonian connecting all interacting vibronic states (36 in total). Such an analysis will be deferred to a future publication.

Here we show that a truncated analysis, that includes only four vibrational levels of the  $V^1\Sigma^+$  state and  $v'=0$  of the  $g^3\Sigma_0^-$  and  $E^1\Sigma^+$  states, is sufficient to explain the main features of the intensity anomaly. For HCl, the levels included were  $v'=8-11$  ( $\nu_{00}=82\,226, 82\,839, 83\,433, \text{ and } 84\,207 \text{ cm}^{-1}$ ), and for DCI the levels were  $v'=12-15$  ( $\nu_{00}=82\,942.2, 83\,389.4, 83\,739, \text{ and } 84\,298 \text{ cm}^{-1}$ ). Parameters in the Hamiltonian include the term values, rotational constants, and rotational distortion constants of the unperturbed electronic states, spin-rotation and spin-spin coupling constants for the  $^3\Sigma^-$  state, spin-orbit interaction constants between the  $^3\Sigma^-$  state and  $V^1\Sigma^+$  and  $E^1\Sigma^+$ , and the electrostatic interaction energy between the  $V$  and  $E$  states. The Hamiltonian was diagonalized, with the unknown pa-

parameters optimized by a least squares fit to the term values of all the observed rotational levels. From the eigenfunctions of the Hamiltonian, we determined the fractional contributions of the zero-order states to the perturbed wave function.

The results of this inversion are plotted in the bottom panels of Figs. 5 and 6. The key to understanding the intensity anomaly is the contribution of the  $V$  state to the total wave function. Since the electronic configuration of this state is  $\sigma\pi^4\sigma^*=(A^2\Sigma^+)3p\sigma^*$ , direct ionization to produce the ground state ion configuration,  $\sigma^2\pi^3=X^2\Pi$ , involves a two-electron change,<sup>25</sup> which is forbidden to first order. By contrast, the configuration of the unperturbed  $E^1\Sigma^+$  Rydberg state is  $(\sigma^2\pi^3)4p\pi$ , and promotion of only one electron ( $4p\pi$ ) to the continuum is required to yield the  $X^2\Pi$  ion core. Although the  $V$  state cannot be ionized by a one-photon process, it *can* be promoted to a predissociated superexcited state.

Both the single-photon ionization of the  $E$  state and the single-photon dissociation of the  $V$  state contribute to the intensity anomaly. Examination of the state characters plotted in the bottom panel of Fig. 6 shows that the total  $V^1\Sigma^+$  contribution to the eigenstate of HCl increases monotonically with  $J'$ , with most of the contribution coming from  $v'=11$ . This trend is in qualitative agreement with the observed intensity anomaly for HCl, which also increases monotonically with  $J'$ . A near qualitative fit of the anomaly, shown in the middle panel of Fig. 6, was obtained with the parameters  $g_{v'=10}\approx 15$ ,  $g_{v'=11}\approx 2$ , and  $p=-1$ . (The sign of  $p$  accounts for interfering contributions from different vibrational levels of the  $V$  state.)

Qualitatively different behavior was found for DCI. In this case, the fraction of  $V^1\Sigma^+$  character is nearly constant for  $J'\leq 7$ . At low  $J'$ ,  $v'=14$ , and  $v'=15$  contribute approximately equally, while at higher  $J'$ ,  $v'=15$  dominates. The decreasing intensity anomaly at high  $J'$  may be understood if  $g_{v'=15}\ll g_{v'=14}$ . The fit shown in the middle panel of Fig. 5, obtained for  $g_{v'=15}\approx 4$ ,  $g_{v'=14}\approx 8$ , and  $p=-1$ , describes well the monotonic decrease in the intensity anomaly at higher  $J'$ . Our determination of  $g>1$  provides a clue as to the identity of the predissociated superexcited state. White *et al.*<sup>42</sup> observed that the autoionization and fluorescence spectra of HCl between 76 and 84 nm do not coincide, indicating that predissociation is at a maximum where the autoionization rate is near a minimum. At the three-photon ( $2+1$ ) energy corresponding to the two-photon  $E-X$  transition, Frohlich *et al.*<sup>43</sup> observed a maximum in the predissociation spectrum, which they assigned to the  $1\Sigma^+[(A^2\Sigma^+)3d\sigma, v'=4]$  level (see Fig. 7 of Ref. 43). Finally, Lefebvre-Brion and Keller<sup>46</sup> showed that this state is predissociated by the  $3\Pi_0[(4\Pi)4s\sigma]$  state.

In conclusion, we have found very different mechanisms for the multiphoton ionization of the  $E$  and  $F$  states of HCl and DCI. The  $F$  state undergoes direct ionization which preserves the ionic core and yields only molecular ions.<sup>36</sup> The intensity anomaly is caused by rotational mixing of the  $F$  state with a predissociated triplet Rydberg state. Predissociation of this state (at the two-photon level) competes with absorption of a third, ionizing photon, resulting in a

$J'$ -dependent intensity loss in the ion yield. The  $E$  state, on the other hand, is mixed with a bound singlet valence state. Absorption of a third photon produces a superexcited state which can either autoionize or predissociate, with the first process deriving from the zero-order Rydberg character of the eigenstate and the second from the valence character. An analogous situation exists in the multiphoton ionization of the  $\text{Na}_2$  molecule. The  $2^1\Pi_g$  state can absorb a photon at its inner turning point to form the molecular ion, or it can absorb a photon near its outer turning point to reach a dissociative state that yields  $\text{Na}+\text{Na}^+$ . The ratio of atomic to molecular ions can be controlled by varying the delay between the pump laser, which populates the  $2^1\Pi_g$  launch state, and the probe laser, which populates the superexcited state.<sup>47</sup>

## ACKNOWLEDGMENTS

This research was supported by the National Science Foundation, under Grants Nos. CHE-9408801 (to R.J.G.) and CHE-9313722 (to P.J.D.), and the U.S. Army Research Office (to P.J.D.), under Grant No. DAAH04-95-1-0128.

<sup>1</sup>For a recent review, see M. N. R. Ashfold, *Annu. Rev. Phys. Chem.* **45**, 57 (1994).

<sup>2</sup>K.-D. Rinnen, D. A. V. Kliner, R. N. Zare, and W. M. Huo, *Isr. J. Chem.* **29**, 369 (1989).

<sup>3</sup>T. A. Spiglanin, D. W. Chandler, and D. H. Parker, *Chem. Phys. Lett.* **137**, 414 (1987).

<sup>4</sup>Y. Xie, P. T. A. Reilly, S. Chilukuri, and R. J. Gordon, *J. Chem. Phys.* **95**, 854 (1991).

<sup>5</sup>R. Liyanage, P. T. A. Reilly, Y. Yang, R. J. Gordon, and R. W. Field, *Chem. Phys. Lett.* **216**, 544 (1993).

<sup>6</sup>D. C. Jacobs, R. J. Madix, and R. N. Zare, *J. Chem. Phys.* **85**, 5469 (1986).

<sup>7</sup>M. A. Hines, H. A. Michelson, and R. N. Zare, *J. Chem. Phys.* **93**, 8557 (1990).

<sup>8</sup>K.-D. Rinnen, M. A. Buntine, D. A. V. Kliner, R. N. Zare, and W. M. Huo, *J. Chem. Phys.* **95**, 214 (1991).

<sup>9</sup>E. A. Rohlfing, D. W. Chandler, and D. H. Parker, *J. Chem. Phys.* **87**, 5229 (1987).

<sup>10</sup>Y. Rudich, R. J. Gordon, E. E. Nikitin, and R. Naaman, *J. Chem. Phys.* **96**, 4423 (1992).

<sup>11</sup>P. T. A. Reilly, Y. Xie, and R. J. Gordon, *Chem. Phys. Lett.* **178**, 511 (1991).

<sup>12</sup>G. He, Y. Yang, Y. Huang, and R. J. Gordon, *J. Phys. Chem.* **97**, 2186 (1993).

<sup>13</sup>Y. Huang, Y. Yang, G. He, and R. J. Gordon, *J. Chem. Phys.* **99**, 2752 (1993).

<sup>14</sup>Y. Huang, G. He, Y. Yang, S. Hashimoto, and R. J. Gordon, *Chem. Phys. Lett.* **229**, 621 (1994).

<sup>15</sup>S.-P. Lu, S.-M. Park, Y. Xie, and R. J. Gordon, *J. Chem. Phys.* **96**, 6613 (1992).

<sup>16</sup>W. R. Simpson, A. J. Orr-Ewing, and R. N. Zare, *Chem. Phys. Lett.* **212**, 163 (1993).

<sup>17</sup>W. R. Simpson, T. P. Rakitzis, S. A. Kandel, A. J. Orr-Ewing, and R. N. Zare, *J. Chem. Phys.* **103**, 7313 (1995).

<sup>18</sup>D. F. Varley and P. J. Dagdigian, *J. Phys. Chem.* **99**, 9843 (1995).

<sup>19</sup>D. F. Varley and P. J. Dagdigian, *J. Phys. Chem.* **100**, 4365 (1996).

<sup>20</sup>Y.-F. Yen, Z. Wang, B. Xue, and B. Koplitz, *J. Phys. Chem.* **98**, 4 (1994).

<sup>21</sup>K. Lykke and B. Kay, in *Laser Photoionization and Desorption Surface Analysis Techniques*, edited by N. S. Nogar (SPIE, Bellingham, 1990), Vol. 1208, p. 18.

<sup>22</sup>C. T. Rettner, *J. Chem. Phys.* **101**, 1529 (1994).

<sup>23</sup>R. Callaghan, S. Arepalli, and R. J. Gordon, *J. Chem. Phys.* **86**, 5273 (1987).

<sup>24</sup>D. S. Green, G. A. Bickel, and S. C. Wallace, *J. Mol. Spectrosc.* **150**, 303 (1991).

<sup>25</sup>D. S. Green and S. C. Wallace, *J. Chem. Phys.* **96**, 5857 (1992).

- <sup>26</sup> See, for example, H. Lefebvre-Brion and R. W. Field, *Perturbations in the Spectra of Diatomic Molecules* (Academic, New York, 1986).
- <sup>27</sup> D. F. Varley and P. J. Dagdigian, *Chem. Phys. Lett.* **255**, 393 (1996).
- <sup>28</sup> J. G. Stamper, *Can. J. Phys.* **40**, 1274 (1962).
- <sup>29</sup> S. G. Tilford, M. L. Ginter, and J. T. Vanderslice, *J. Mol. Spectrosc.* **33**, 505 (1970).
- <sup>30</sup> S. G. Tilford and M. L. Ginter, *Mol. Spectrosc.* **40**, 568 (1971).
- <sup>31</sup> K. P. Huber and F. Alberti, *J. Mol. Spectrosc.* **97**, 387 (1983).
- <sup>32</sup> A. E. Douglas and F. R. Greening, *Can. J. Phys.* **57**, 1650 (1979).
- <sup>33</sup> J. A. Coxon, H. G. Hajigeorgiou, and K. P. Huber, *J. Mol. Spectrosc.* **131**, 288 (1988).
- <sup>34</sup> A. Arepalli, N. Presser, D. Robie, and R. J. Gordon, *Chem. Phys. Lett.* **118**, 88 (1985).
- <sup>35</sup> E. de Beer, B. G. Koenders, M. P. Koopmans, and C. A. de Lange, *J. Chem. Soc. Faraday Trans.* **86**, 2035 (1990).
- <sup>36</sup> E. de Beer, W. J. Buma, and C. de Lange, *J. Chem. Phys.* **99**, 3252 (1993).
- <sup>37</sup> W. C. Wiley and I. H. McLaren, *Rev. Sci. Instrum.* **26**, 1150 (1955).
- <sup>38</sup> D. H. Rank, D. P. Eastman, B. S. Rao, and T. A. Wiggins, *J. Opt. Soc. Am.* **52**, 1 (1962).
- <sup>39</sup> K. P. Huber and G. Herzberg, *Molecular Spectra and Molecular Structure IV. Constants of Diatomic Molecules* (Van Nostrand Reinhold, New York, 1979).
- <sup>40</sup> R. G. Bray and R. M. Hochstrasser, *Mol. Phys.* **31**, 1199 (1976).
- <sup>41</sup> A. C. Kummel, G. O. Sitz, and R. N. Zare, *J. Chem. Phys.* **85**, 6874 (1986).
- <sup>42</sup> M. G. White, G. E. Leroy, M.-H. Ho, and E. D. Poliakoff, *J. Chem. Phys.* **87**, 6553 (1987).
- <sup>43</sup> H. Frohlich and M. Glass-Maujean, *Phys. Rev. A* **42**, 1396 (1990).
- <sup>44</sup> These coefficients were estimated by diagonalizing a  $2 \times 2$  spin-orbit Hamiltonian. See, for example, in Ref. 26, pp. 248–251.
- <sup>45</sup> Caution should be used in comparing the fitted values of  $g_2$  for different transitions. The assumption that  $g_2$  is independent of laser intensity is based on the saturation of the ionization step in the 2+1 REMPI spectrum of DCI displayed in Fig. 2(a). Such measurements were not undertaken for all the reported transitions, and even where they were carried out, a very wide range of intensities was not investigated. Although the fitted values of  $g_2$  should therefore be regarded as phenomenological constants, the general trends reported are still meaningful. Similar caution should also be exercised in using the correction factors in Tables IV–VII at intensities very different from those employed in this study. In practice, this should not cause serious difficulty, since one would not normally use higher intensities, so as to avoid saturation of the two-photon resonant transition.
- <sup>46</sup> H. Lefebvre-Brion and F. Keller, *J. Chem. Phys.* **90**, 7176 (1989).
- <sup>47</sup> T. Baumert, R. Thalweiser, V. Weiss, and G. Gerber, in *Femtosecond Chemistry*, edited by J. Manz and L. Wöste (VCH, Weinheim, 1995), p. 397.